Sensing RISs: Enabling Dimension-Independent CSI Acquisition for Beamforming

Jieao Zhu, Kunzan Liu, Zhongzhichao Wan, Linglong Dai, *Fellow, IEEE*, Tie Jun Cui, *Fellow, IEEE*, and H. Vincent Poor, *Life Fellow, IEEE*

Abstract

Reconfigurable intelligent surfaces (RISs) are envisioned as a potentially transformative technology for future wireless communications. However, RIS's inability to process signals and their attendant increased channel dimension have brought new challenges to RIS-assisted systems, which greatly increases the pilot overhead required for channel estimation. To address these problems, several prior contributions that enhance the hardware architecture of RISs or develop algorithms to exploit the channels' mathematical properties have been made, where the required pilot overhead is reduced to be proportional to the number of RIS elements. In this paper, we propose a dimension-independent channel state information (CSI) acquisition approach in which the required pilot overhead is independent of the number of RIS elements. Specifically, in contrast to traditional signal transmission methods, where signals from the base station (BS) and the users are transmitted in different time slots, we propose a novel method in which signals are transmitted from the BS and the user simultaneously during CSI acquisition. Under this method, an electromagnetic interference random field (IRF) will be induced on the RIS, and we employ a sensing RIS to capture its features. Moreover, we develop three algorithms for parameter estimation in this system, and also derive the Cramér-Rao lower bound (CRLB) and an asymptotic expression for it. Simulation results verify that our proposed signal transmission method and the corresponding algorithms can achieve dimension-independent CSI acquisition for beamforming.

Index Terms

J. Zhu, K. Liu, Z. Wan, and L. Dai are with the Beijing National Research Center for Information Science and Technology (BNRist) as well as the Department of Electronic Engineering, Tsinghua University, Beijing 100084, China (e-mails: {zja21, lkz18, wzzc20}@mails.tsinghua.edu.cn, daill@tsinghua.edu.cn).

T. J. Cui is with the State Key Laboratory of Millimeter Waves, Southeast University, China (e-mail: tjcui@seu.edu.cn).

H. V. Poor is with the Department of Electrical and Computer Engineering, Princeton University, USA (e-mail: poor@princeton.edu).

This work was supported in part by the National Key Research and Development Program of China (Grant No.2020YFB1807201), in part by the National Natural Science Foundation of China (Grant No. 62031019), and in part by the European Commission through the H2020-MSCA-ITN META WIRELESS Research Project (Grant No. 956256).

Reconfigurable intelligent surface (RIS), channel estimation, interference random field (IRF), dimension-independent CSI acquisition.

I. Introduction

Reconfigurable intelligent surfaces (RISs) are considered to be a potentially important technology for future wireless communications. The characteristics of low cost and power consumption make RISs a promising solution for overcoming blockages, improving capacity, and reducing transmit power [1]–[3]. Specifically, an RIS is a large-scale array composed of passive elements, which can achieve significant beamforming gain by appropriately imposing phase shifts on the incident electromagnetic waves [4]. To achieve this beamforming gain, accurate channel state information (CSI) should be acquired beforehand, which makes channel estimation an essential problem for RIS-assisted communications [5].

Although channel estimation has been well investigated in conventional communication systems, the additional employment of RISs brings about two challenges [6]. Firstly, in contrast to traditional antenna array capable of transmitting, receiving, and processing the signals, RISs can only passively reflect the incident signals. Secondly, since the number of RIS elements is usually large, the dimensions of the channels increase sharply compared with conventional communication systems, which results in unacceptably high pilot overhead for channel estimation. These two main challenges result in the need for new channel estimation techniques for beamforming in RIS-assisted communications.

A. Prior Works

Generally, for RIS-assisted systems, channel estimation and beamforming are two separate procedures. Channel estimation is performed first, and then the obtained CSI is utilized for beamforming. The beamforming gain relies heavily on the channel estimation accuracy.

To tackle the challenges mentioned above in channel estimation for RIS-assisted communications, some solutions have been proposed, which can be generally divided into two categories. The first category modifies the hardware architecture of the RIS, which enables some signal processing capability. For example, by sparsely replacing some of the RIS elements with active sensors capable of baseband processing, the authors of [7] proposed a compressive sensing and deep learning-based channel estimation scheme with negligible pilot overhead. To further reduce the number of active sensors, in [8] the authors proposed an alternating direction method-based

channel estimation procedure with a single radio-frequency (RF) chain, with the help of an extended analog combiner [9]. Since RF chains have been attached to RISs for channel sensing in these works, they can also be modified to perform signal relaying. In [10], a hybrid relay-reflecting architecture is considered, where a few passive RIS elements are replaced by active amplify-and-forward relay modules. These active modules are then capable of channel estimation.

The second category preserves the original hardware architecture of RISs, while conceiving new algorithms to exploit the specific features that RISs bring about. Exploiting the two-timescale channel property in the RIS-assisted system, the authors of [11] proposed a two-timescale channel estimation algorithm that reduces the pilot overhead in the time-averaged sense. In other works [5], [12], by exploiting the sparsity of channels in the angular domain, compressive sensing-based algorithms are developed with reduced pilot overhead. In [13], based on the shared reflected channels among multiple users, the authors proposed a three-phase channel estimation framework to further reduce the pilot overhead.

Note that, in order to achieve high beamforming gain, all the above channel estimation methods are designed to estimate the full channel matrix as accurately as possible. However, since the channel matrix is at least of size $\mathcal{O}(N)$, where N denotes the number of RIS elements, the required pilot overhead for channel estimation is usually proportional to the number of RIS elements [7]–[14] in practical systems, which makes most of the existing channel estimation schemes dimension-dependent. This is unacceptable especially when the RIS is fabricated with a large number of elements (e.g. 1100 elements in [15], 2304 elements in [16], and 10240 elements in [17]). Therefore, the following question naturally arises: *Does there exist a dimension-independent approach where the required pilot overhead is independent of the number of RIS elements?*

B. Our Contributions

We point out that the main drawback of conventional channel estimation methods is that they only extract the mathematical features of channels, while neglecting their electromagnetic nature. This limitation has caused the problem of high pilot overhead required for channel estimation in RIS-assisted systems. Thus, we propose an interference random field (IRF)-based approach, where the IRF induced on an RIS is utilized for channel estimation[1]. Specifically, the

[1]Simulation codes will be provided to reproduce the results in this paper: http://oa.ee.tsinghua.edu.cn/dailinglong/publications/publications.html.

contributions of this paper can be summarized as follows.

- Inspired by optical interference where phase information can be obtained from the interference fringes, we reveal that phase information about the channel can also be gathered from the phenomenon of electromagnetic interference that occurs on RISs, which we name the IRF. To induce the IRF on an RIS, we propose a novel pilot transmission method called simultaneous rotational signaling, where signals are transmitted from the base station (BS) and the user to the RIS simultaneously, and the two signals bear a slight frequency difference during CSI acquisition.
- To exploit this IRF for CSI acquisition, we employ a sensing RIS that integrates power detectors into the RIS elements to capture the features of the IRF. Each of the power detectors can acquire its phase information independently from the IRF, so that the required pilot overhead is independent of the number of RIS elements. We then develop discrete Fourier transform (DFT), maximum likelihood (ML), and von Mises-expectation maximization (VM-EM) phase estimation algorithms to extract the phase information from the power detector signals in order to perform beamforming.
- We derive the Cramér-Rao lower bound (CRLB) of the phase estimation problem based on the IRF, and its approximated asymptotic expression for channel estimation in the sensing RIS-assisted system. Our numerical results verify that this approximated CRLB is asymptotically precise, and that our developed algorithms are close to the CRLB. Our simulation results further demonstrate that our proposed signal transmission method and the corresponding algorithms can realize dimension-independent CSI acquisition for beamforming, and then achieve near-optimal spectral efficiency.

C. Organization and notation

Organization: The rest of the paper is organized as follows. In Section II, we introduce the system model of RIS-aided communications, and review the existing separate procedures of beamforming and channel estimation. In Section III, we propose a novel signal transmission method for CSI acquisition in RIS-aided system, and reveal the IRF phenomenon under this method. In Section IV, we introduce the hardware architecture of a sensing RIS to exploit the IRF. Based on the sensing RIS, we propose three algorithms to realize channel estimation. In Section VI, we derive the CRLB and its asymptotic expression for channel estimation in the sensing RIS-assisted system. In Section VII, simulation results are provided for quantifying the

performance of our proposed sensing RIS-based channel estimation as a dimension-independent approach. Finally, in Section VIII, we provide our conclusions followed by promising future research ideas.

Notation: $\mathbb{C}$ and $\mathbb{R}$ denote the set of complex and real numbers, respectively; $\{L\}$ represents the set of integers $\{0, 1, \cdots, L-1\}$; $\boldsymbol{A}^{-1}, \boldsymbol{A}^{*}, \boldsymbol{A}^{T}$, and $\boldsymbol{A}^{H}$ denote the inverse, conjugate, transpose, and conjugate transpose of matrix $\boldsymbol{A}$, respectively; $\|\cdot\|_2$ is the $\mathcal{L}_2$-norm of its argument function; $\|\cdot\|_F$ denotes the Frobenius norm of its argument matrix; $\arg(x)$ and $\exp(x)$ denote the phase angle and exponential representation of the complex scalar x, respectively; $|x|$ denotes the amplitude of a complex scalar x; $\text{diag}(\cdot)$ is the diagonal operation; $\mathcal{CN}(\mu, \sigma^2)$ represents the complex univariate Gaussian distribution with the mean μ and the variance σ^2; $\mathcal{VM}(\mu, \kappa)$ denotes the von Mises distribution with circular mean $\mu \in [0, 2\pi]$ and centrality κ; $\mathcal{NC}_{\chi_k^2}(\lambda, \sigma^2)$ and $\mathcal{NC}_{\chi_k}(\lambda)$ are the degree-k non-central chi-squared distribution with non-centrality parameter λ and variance parameter σ^2, and the non-central chi distribution with non-centrality parameter λ, respectively; $\boldsymbol{I}_L$ denotes the $L \times L$ identity matrix; $x_{\text{BB}}(t)$ denotes the baseband representation of a passband signal $x(t)$; $I_\nu(z)$ is the ν-th order modified Bessel function of the first kind.

II. System Model

In this section, we will first specify the system model of the RIS-assisted multiple-input single-output (MISO) system. Then, we will introduce traditional approaches for the corresponding beamforming design and channel estimation in Subsection II-A and II-B, respectively.

Let us consider an RIS-aided MISO system, where an N-element RIS is employed for enhancing the transmission from an M-antenna BS to a single-antenna user. Assume furthermore that the phase-shift of each element of the RIS can be continuously and independently controlled [3]. Then, the precoding matrix of the RIS can be represented by $\boldsymbol{\Theta} = \text{diag}(\boldsymbol{\theta}) = \text{diag}\left([\theta_1, \cdots, \theta_N]^T\right)$, where $\theta_n (n \in \{N\})$ denotes the phase-shift of the n-th RIS element, satisfying $|\theta_n| = 1$. Therefore, the signal received by the user can be written as

$$y = \boldsymbol{f}^H \boldsymbol{\Theta} \boldsymbol{G} \boldsymbol{w} s + z, \tag{1}$$

where $\boldsymbol{f} \in \mathbb{C}^{N \times 1}$ and $\boldsymbol{G} \in \mathbb{C}^{N \times M}$ denote the channel spanning from the RIS to the user and the channel spanning from the BS to the RIS, respectively; $\boldsymbol{w} \in \mathbb{C}^{M \times 1}$ denotes the beamforming vector at the transmitter BS, with power constraint $\|\boldsymbol{w}\|_2^2 \leq P_{\text{max}}$; s denotes the normalized BS transmitted symbol; $z \sim \mathcal{CN}(0, \sigma_z^2)$ denotes the additive white Gaussian noise (AWGN)

introduced at the receiver user. To focus on RIS beamforming, other possible links are neglected in this paper[2].

A. Beamforming Design

Based on the received signal (1), we can formulate the signal-to-noise ratio (SNR) maximization problem for designing the beamforming vector $\boldsymbol{w}$ and precoding matrix $\boldsymbol{\Theta}$, i.e.,

$$\max_{\boldsymbol{\Theta}} \quad \text{SNR} = \frac{1}{\sigma_z^2}\left|\boldsymbol{f}^H\boldsymbol{\Theta}\boldsymbol{G}\boldsymbol{w}\right|^2, \tag{2a}$$

$$\text{s.t.} \quad \text{C}_1 : \|\boldsymbol{w}\|_2^2 \le P_{\max}, \tag{2b}$$

$$\text{C}_2 : |\theta_n| = 1, \ \forall n. \tag{2c}$$

In this paper, we assume that the locations of the BS and the RIS are unchanged, which can provide us a beamforming approach expressed as

$$\boldsymbol{w} = \sqrt{P_{\max}}\boldsymbol{a}\left(\alpha\right), \quad \theta_n = \exp\left(-\text{jarg}\left(f_n^*\boldsymbol{g}_n^T\boldsymbol{w}\right)\right), \ \forall n \in \{N\}, \tag{3}$$

where $\boldsymbol{a}(\alpha)$ denotes the array steering vector with respect to the wave departure angle α of the BS antenna array, and $\boldsymbol{G} = \left[\boldsymbol{g}_1, \cdots, \boldsymbol{g}_N\right]^T$.

B. Channel Estimation

Observe from (3) that, the estimation for the cascade channel $\boldsymbol{H} = \text{diag}(\boldsymbol{f}^*)\boldsymbol{G}$ is enough for beamforming design. To accurately acquire this cascade channel, the user generally sends pilot signal x to the BS under P different RIS configurations which are the first P columns of the DFT matrix $\boldsymbol{F}_N$, denoted as $\boldsymbol{F}_{N,P}$. Due to the channel reciprocity, the received signal at the BS with the p-th RIS configuration $\boldsymbol{\Theta}_p = \text{diag}(\boldsymbol{\theta}_p)$ can be written as [18]

$$\boldsymbol{y}_{\text{BS},p} = \boldsymbol{H}^T\boldsymbol{\theta}_p w' s' + \boldsymbol{n}, \tag{4}$$

where w' is the precoding scalar of the user satisfying $|w'|^2 \le P'_{\max}$, s' is the normalized user transmitted symbol, and $\boldsymbol{n} \sim \mathcal{CN}\left(\boldsymbol{0}_M, \sigma_n^2\boldsymbol{I}_M\right)$ is the AWGN at the receiver BS. Equivalently,

[2]In fact, our proposed CSI acquisition procedure automatically works when there exists extra links, which will be explained later in this paper.

(4) can be expressed in the matrix form

$$\boldsymbol{Y}_{\mathrm{BS}} = \boldsymbol{H}^T \boldsymbol{F}_{N,P} w' s' + \boldsymbol{N}, \tag{5}$$

where $\boldsymbol{Y}_{\mathrm{BS}} = [\boldsymbol{y}_{\mathrm{BS},1}, \cdots, \boldsymbol{y}_{\mathrm{BS},P}]$ and $\boldsymbol{N} = [\boldsymbol{n}_1, \cdots, \boldsymbol{n}_P]$. Given the received signal $\boldsymbol{Y}_{\mathrm{BS}}$ and, without loss of generality, assuming $w's' = 1$, the channel estimation problem in RIS-assisted system can be formulated as

$$\hat{\boldsymbol{H}} = \arg\min_{\boldsymbol{H}} \|\boldsymbol{Y}_{\mathrm{BS}} - \boldsymbol{H}^T \boldsymbol{F}_{N,P}\|_F^2. \tag{6}$$

With the least-square (LS) criterion [14], we obtain

$$\hat{\boldsymbol{H}}_{\mathrm{LS}} = \frac{1}{P} \boldsymbol{F}_{N,P}^* \boldsymbol{Y}_{\mathrm{BS}}^T, \tag{7}$$

which provides a feasible solution to channel estimation in this RIS-assisted MISO system. In this paper, we name it the least-square channel estimation (LS-CE) method.

III. Interference Random Field

In this section, the signal model for the IRF will be first introduced in Subsection III-A. Then, in order to acquire the CSI, the simultaneous rotational signaling method will be proposed in Subsection III-B.

A. Signal Model for IRF

Physical intuition is vital in designing RIS-aided systems [19], and interference is a fundamental physical phenomenon in all kinds of waves. The most well-known example is the double-slit optical interference [20], as is shown in Fig. 1 (a), where the interference fringes created during the wave superposition reveal the phase difference of the two optical paths. Similarly, the same interference phenomenon occurs when two RF electromagnetic waves meet together on the RIS, as is shown in Fig. 1 (b), and the IRF created by this interference reveals the CSI.

Suppose two signals impinge upon the RIS simultaneously, creating an interference field at the n-th RIS element. Denote the symbol transmitted from the BS by s, and the symbol transmitted from the user by s'. In order to perform channel estimation by exploiting the IRF, we need to probe the interference fringes, i.e., the power of the IRF. To clarify the power problem associated with an electromagnetic signal, the relationship between physical signal power and

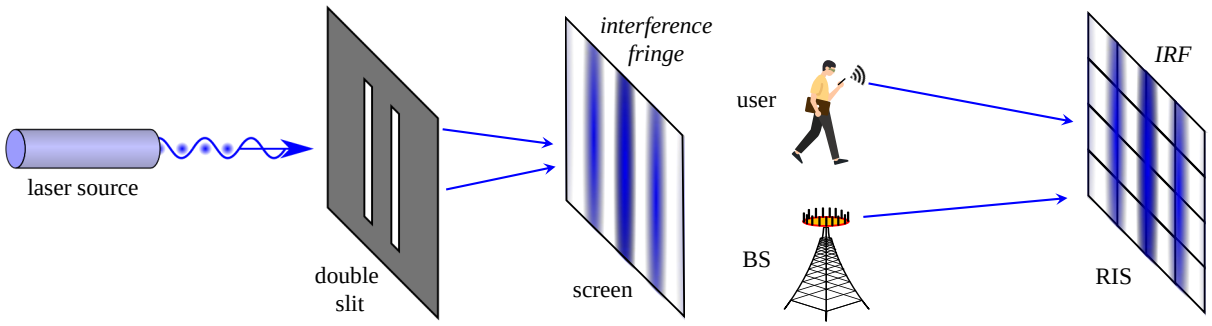

(a) Optical interference. (b) Electromagnetic interference.

Fig. 1. Analogy between the optical interference and the IRF phenomenon induced on the RIS.

baseband equivalent signal power is stressed in the following formulas. If we represent both of the BS-RIS and user-RIS signals that appear on each RIS element by their baseband equivalent signals $E_{\mathrm{BB}}(t)$, then the corresponding physical passband electric field induced on each RIS element is characterized by

$$E(t) = \sqrt{2}\Re\left(E_{\mathrm{BB}}(t)e^{\mathrm{j}\omega_c t}\right), \tag{8}$$

where $\omega_c = 2\pi f_c$ denotes the carrier frequency, and the coefficient $\sqrt{2}$ ensures that the passband signal power is equal to the baseband signal power, i.e., $\|E_{\mathrm{BB}}\|_2^2 = \|E\|_2^2$. Thus, taking the square of the baseband signal is equivalent to calculating the power of the physical electromagnetic signal. Now we consider the IRF case, where a superposition of the BS-RIS signal and the user-RIS signal is considered. Following the notations in Section II and due to the linearity of (8), we obtain the noisy IRF signal by adding up the two impinging baseband signals

$$\begin{aligned} E_{\mathrm{BB,IRF}}(t) &= E_{\mathrm{BB,BS}}(t) + E_{\mathrm{BB,user}}(t) + v(t) \\ &= \boldsymbol{g}_n^T \boldsymbol{w} s + f_n^* w' s' + v(t), \end{aligned} \tag{9}$$

where $v(t) \sim \mathcal{CN}(0, \sigma_v^2)$ is the electromagnetic noise signal in its baseband representation, $\boldsymbol{w}$ and w' are the beamforming vector at the BS side and the user side satisfying $\|\boldsymbol{w}\|_2^2 \leq P_{\max}$ and $|w'|^2 \leq P'_{\max}$, respectively, s is the symbol transmitted from the BS to RIS, and $s' = e^{\mathrm{j}\psi(t)}$ is the time-varying transmitted symbol from the user to the RIS. Since the interference fringes are not sensitive to a global phase change, we can safely assume that $s = 1$, and then the relative phase between the user and the BS can be fully characterized by a time-varying phase function $\psi(t)$.

Furthermore, by defining $\alpha = \left|\boldsymbol{g}_n^T \boldsymbol{w}\right|$, $\beta = |f_n^* w'|$, and the phase difference between the BS-

RIS link[3] and the RIS-user channel as $\varphi = \arg\left(f_n^* w'\right) - \arg\left(\boldsymbol{g}_n^T \boldsymbol{w}\right)$, then the power of the IRF can be written as

$$\begin{aligned} P(t) &= A\left|E_{\mathrm{BB,IRF}}(t)\right|^2 + \zeta \\ &= \underbrace{A\left[\alpha^2 + \beta^2 + 2\alpha\beta\cos\left(\psi(t)+\varphi\right)\right]}_{\text{IRF power signal}} + \underbrace{2A\Re\left\{\left(\alpha + \beta e^{\mathrm{j}(\psi(t)+\varphi)}\right) v'^*(t)\right\} + A\left|v'(t)\right|^2 + \zeta}_{\text{Noise}}, \end{aligned} \tag{10}$$

where ζ is the noise introduced by digital signal processing after measuring the IRF power, A is the amplification factor of the power sensor, and the equivalent electromagnetic noise $v'(t) = e^{\mathrm{j}\arg(\boldsymbol{g}_n^T \boldsymbol{w})} v^*(t)$ follows the same distribution as $v(t)$ for any time t. The name IRF comes from the randomness of the unknown φ, the unknown noise realization, and the interferential nature of the field.

The phase difference φ defined here will play an important role in our following channel estimation, since it carries enough CSI for beamforming, which will be justified in the next section. To estimate the phase difference φ, we need enough observations from the sensor-detected power signal $P(t)$. For simplicity and without loss of generality, we can assume $\psi(t) = \frac{2\pi}{T_s} t$, where T_s is the symbol period. Furthermore, assume that L observations $P[l] = P(t_l)$ located at equally-spaced instants $t_l = \frac{l}{L} T_s$ for all $l \in \{L\}$ are used for phase estimation φ.

B. Simultaneous Rotational Signaling and Interference Detection

However, at first glance it seems impractical to use only power signals to obtain enough information for RIS beamforming, in the absence of phase information. Generally, signal processing with only amplitude signals are called *noncoherent* detection. The target of RIS beamforming is to strengthen the signal at the user, hence it requires *coherent* signal combining at the user antenna. As a result, for *noncoherent* detection, it seems that the lack of phase information makes beamforming impossible. Fortunately, the physical phenomenon *interference* makes it possible to convert phase difference into intensity difference, allowing *noncoherent* devices to perform *coherent* detection.

To clarify this idea, we take only one RIS element into consideration. As is introduced in the previous subsection, if we allow the BS and the user to transmit electromagnetic waves

[3]Since it is usually difficult to obtain the optimal BS beamforming vector $\boldsymbol{w}$, during the CSI acquisition procedure, we fix $\boldsymbol{w}$ to a steering vector that guides most of the signal energy to the RIS aperture. As a result, $\boldsymbol{g}_n^T \boldsymbol{w}$ can be treated as the equivalent link seen by the symbol s.

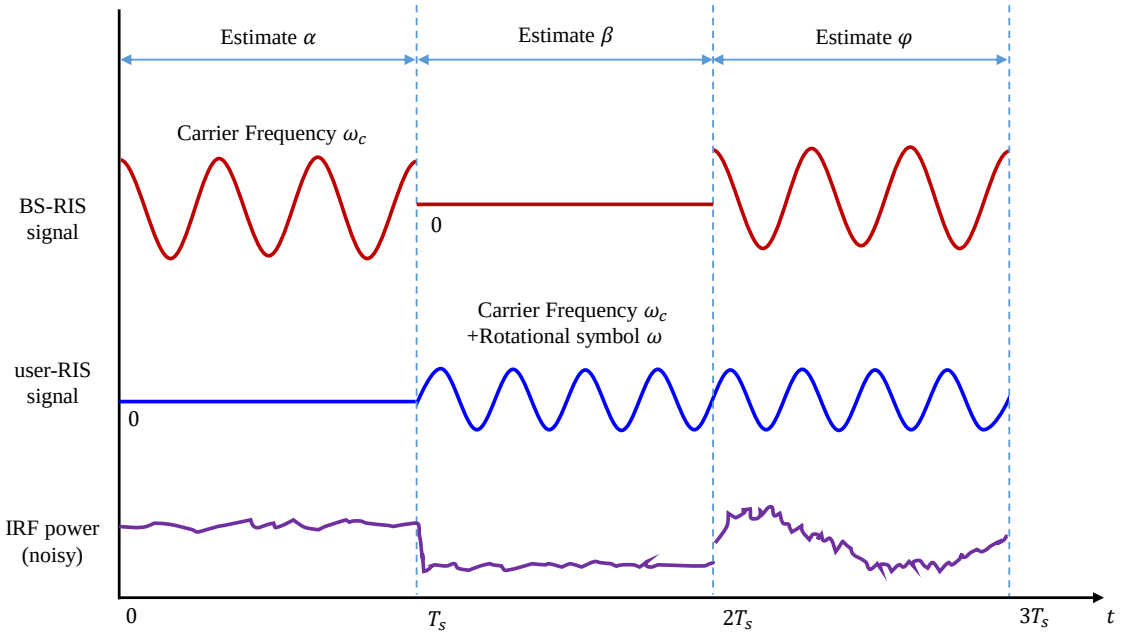

Fig. 2. Simultaneous rotational signaling scheme. The IRF power is the instantaneous total power of the BS-RIS signal and the user-RIS signal. The composite power waveform that appears on RIS enables our algorithm to obtain the desired CSI. The parameters α and β are estimated from the signals $P_\alpha(t), P_\beta(t)$ measured during the first two time slots, and φ is estimated by IRF signal $P(t)$ that occurs during the third time slot.

simultaneously, then the interference phenomenon will occur on each RIS element. However, equal carrier frequencies of the BS and the user create stable interference fringes [20] on the RIS, which do not carry information about the channel. In contrast, a rotational symbol $s' = e^{\mathrm{j}\psi(t)}$ at the user, which is equivalent to a slightly higher carrier frequency, enables the IRF power to vary over time. Thus, the desired CSI can be drawn from the varying IRF power signal received by sensing RIS. Fig. 2 shows the simultaneous rotational signaling procedure and the IRF waveform.

To further analyze the interference, we focus on the received IRF signal $P(t)$ of the n-th RIS element. Note that the power of interference field measured at instant t, expressed by (10), exhibits a sinusoidal waveform in the time domain, as is shown in Fig. 3. The initial phase ($t = 0$) of this sinusoidal waveform is uniquely determined by φ. Thus, if we have access to the power received by the n-th element at successive instants t_l, it is possible to retrieve the phase difference φ. However, according to (3), it is the phase sum of the RIS-user channel and the BS-RIS channel, i.e., $\arg(\boldsymbol{g}_n^T\boldsymbol{w}) + \arg(f_n^* w')$, that determines the optimal phase-shift of the n-th element. Given the phase difference $\varphi = \arg\left(f_n^* w'\right) - \arg\left(\boldsymbol{g}_n^T\boldsymbol{w}\right)$, we assume the phase

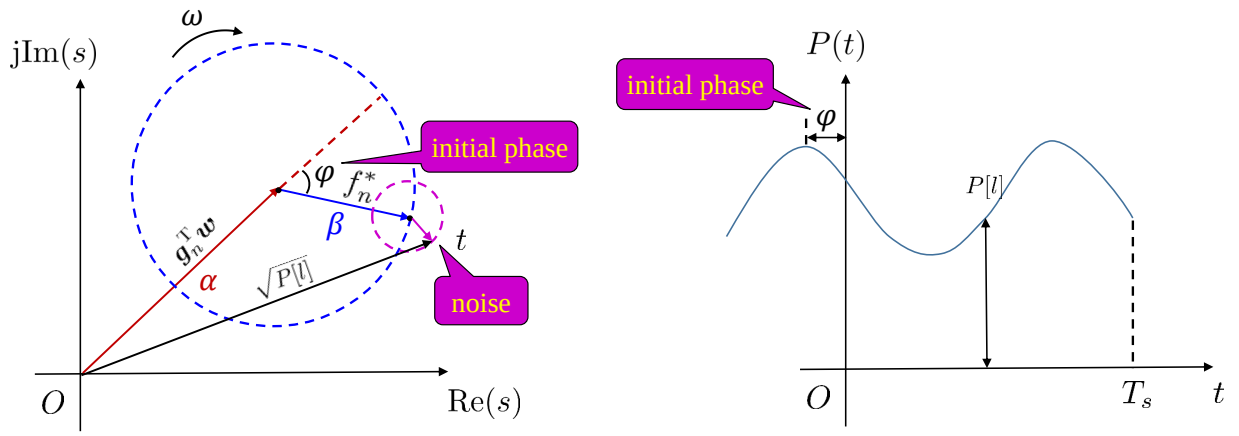

Fig. 3. Phasor representation of the IRF on each RIS element. Red vector represents the complex BS-RIS signal $\boldsymbol{g}_n^T\boldsymbol{w}$; Blue vector represents the complex user-RIS signal $f_n^* w'$; α and β denote the amplitude of these signals respectively. In our signaling method, the BS transmits a fixed symbol $s = 1$, while the user transmits a rotating symbol $s' = e^{\mathrm{j}\psi(t)}$, causing the output of the power sensor $P(t)$ to vary in a waveform that is similar to a sine curve.

$\arg(\boldsymbol{g}_n^T\boldsymbol{w})$ to be known in our algorithms in order to acquire the phase sum. This is because, in contrast to the fast time-varying RIS-user link, the BS-RIS link often exhibits a quasi-static property, which provides an opportunity to simplify the phase estimation [11]. In practice and our simulations, the phase $\arg(\boldsymbol{g}_n^T\boldsymbol{w})$ is calculated based on the geometry, i.e., the locations of the BS and the RIS [21].

IV. Sensing RIS-Based Channel Estimation

In this section, we will first briefly introduce the hardware architecture required for detecting the IRF in Subsection IV-A. Then, the core concept of IRF channel estimation and beamforming procedures will be introduced in Subsection IV-B. Finally, Subsection IV-C will include the analysis on pilot overhead and computational complexity of our proposed IRF-based CSI acquisition methods.

A. Hardware Architecture of Sensing RIS

To obtain the amplitude of the induced IRF, inspired by the sensing metasurface [22], we propose a hardware architecture named sensing RIS. In contrast to traditional RIS architecture shown in Fig. 4 (a), where each RIS element includes a phase-shift circuit and a patch antenna, each sensing RIS element additionally integrates a power sensor which is responsible for detecting the amplitude of the IRF [23], as shown in Fig. 4 (b). Since all of the RIS elements

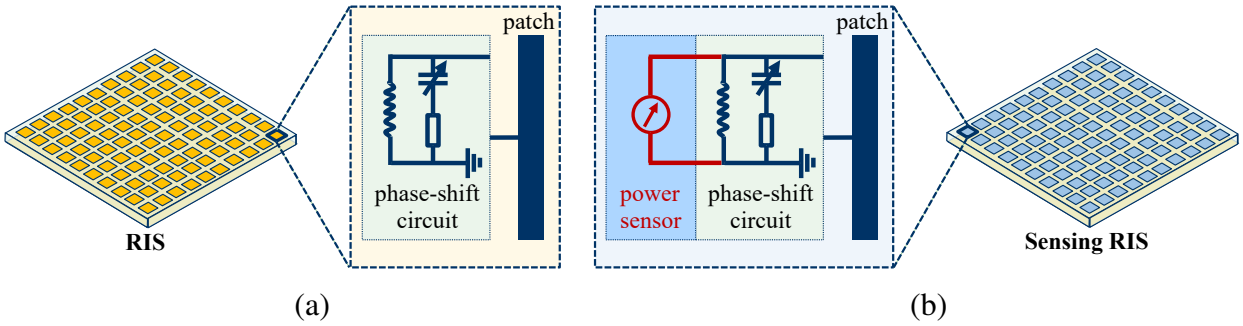

Fig. 4. Comparison of hardware architectures. (a) Traditional RIS. (b) Proposed sensing RIS.

can sense and adjust the phase independently from one another, low-cost microcontroller units (MCUs) can be attached locally to each RIS element to allow parallel computation of the optimal phases. However, for extremely large-scale RIS systems, sparse sensing and controlling may be preferred to reduce cost and hardware complexity.

B. IRF Channel Estimation and Beamforming

In this subsection, we will thoroughly introduce the IRF-based algorithms for adjusting the phases of the RIS elements. The IRF channel estimation and beamforming procedure can be divided into three steps:

1) Simultaneous rotational signaling and power sensing;
2) Phase estimation based on power data;
3) Integrate phase information and other CSI to perform beamforming.

In step 1), three power signals are recorded: $P_\alpha(t)$, $P_\beta(t)$, and $P(t)$. The IRF appears during the third signal $P(t)$. In order to create an IRF, simultaneous rotational signaling must be performed. In fact, the signaling requirements can be realized by transmitting a symbol $s = 1$ on the zeroth subcarrier at the BS, while transmitting a symbol $s' = 1$ on the k-th subcarrier at the user. As is mentioned above, if we denote the OFDM symbol period by T_s, then the equivalent IRF angular frequency ω is given by $\omega = 2\pi k/T_s$, which means the noiseless power signal exhibits exactly k sinusoidal periods during an OFDM symbol. For calculation simplicity, in this paper, we always assume $k = 1$. In fact, for multi-user MISO systems[4], different k values can be assigned to

[4]In this paper, we assume that the user is equipped with a single antenna, but the number of antennas at BS is not restricted. Furthermore, for MIMO systems, since the user is equipped with multiple antennas, phase-tuning simply for constructive interference at the user is sub-optimal. Thus, IRF methods should be further improved to fully harness the space-multiplexing gains of MIMO.

different users in order to enable channel estimation and beamforming design for several users within a single OFDM symbol. This can be done by Fourier analysis on the power signal $P(t)$ and extraction of phase angles for each user at distinct frequencies.

The second step 2) is called *phase estimation*. This step is designed to extract the phase difference φ between the BS-RIS and RIS-user channel. This is the key step of dimension-independent IRF channel estimation and beamforming, since this step can be done independently among all the RIS elements.

The third step 3) is to utilize the phase information provided by step 2) and calculate the near-optimal phase shifts for each RIS element in order to perform beamforming. The additional CSI refers to the phase information $\arg(\boldsymbol{g}_n^T\boldsymbol{w})$.

Step 2) and step 3) are executed by processors, so we collect these two steps into pseudo codes shown in **Algorithm 1**:

Algorithm 1 Near-optimal RIS Beamforming by IRF

Input: Number of RIS elements N, IRF power signals detected on each RIS element $P_\alpha(t), P_\beta(t)$ and $P(t)$.

Output: RIS phase-shift matrix $\boldsymbol{\Theta}$.

for $n = 1, 2, \cdots, N$ **do**
  Estimate α and β from $P_\alpha(t)$ and $P_\beta(t)$.
  Estimate phase difference φ_n from $P(t)$, α and β.
  Estimate $\psi_n = \arg(\boldsymbol{g}_n^T\boldsymbol{w})$ from known locations of BS and RIS
  $\theta_n \leftarrow \exp(-\mathrm{j}(\varphi_n + 2\psi_n))$
end for
$\boldsymbol{\Theta} \leftarrow \mathrm{diag}\left([\theta_1, \theta_2, \cdots, \theta_N]^T\right)$
return $\boldsymbol{\Theta}$

Note that in each iteration n of **Algorithm 1**, the data $P(t)$ is independent of other iterations. Thus, we can perform the calculations in parallel for each phase-shift θ_n. For example, we can install an MCU for each of the elements on the RIS. Each MCU is only responsible for gathering the data from its own power sensor and adjusting the phase-shift of its own RIS element. Since all MCUs can work in parallel, the computational time is independent of the number of RIS elements, resulting in an $\mathcal{O}(1)$ time complexity.

TABLE I
PILOT OVERHEAD COMPARISON OF DIFFERENT CSI ACQUISITION METHODS

CSI acquisition method	Minimum pilot overhead	Type of RIS	Channel assumption
MVU [25]	$NK + K$	RIS	General
Multi-user [13]	$K + N + \lceil \frac{(K-1)N}{M} \rceil$	RIS	General
CS [5]	$\mathcal{O}(KS \log N)$	RIS	Sparse
Two-timescale [11]	$\frac{2(N+1)}{\alpha} + K\lceil N/M \rceil + K$	RIS	Quasi-static BS-RIS
Proposed IRF	3	Sensing RIS	Quasi-static BS-RIS

C. Pilot Overhead and Computational Complexity

In our proposed IRF-based CSI acquisition method, the pilot overhead is fixed to $\mathcal{O}(1)$, which is independent of the RIS dimension N. The reason is that, no matter how many RIS elements are employed, the IRF appears on them simultaneously. Thus, both the channel estimation and beamforming can be fulfilled within only three pilot symbols, as is depicted in Fig. 2. Thus, the pilot overhead is independent of the RIS dimension N. To the best of our knowledge, this dimension-independent property is unprecedented, if we cannot endure the cost of attaching a dedicated RF chain to every RIS element. Some hybrid solutions do exist, such as connecting all the RIS elements to several RF chains with analog combiners [8], [24] to enable explicit channel estimation at RIS. Unfortunately, the cost of analog combiners and RF chains are usually higher than power sensors.

Table I compares the pilot overhead of our proposed IRF method with other different CSI acquisition methods. K denotes the number of users, S is the sparsity of the channel assumption, M is the number of antennas at BS, and α is the ratio of the large-timescale channel coherence time and the small-timescale channel coherence time [11]. Except for CS-based methods [5], all the channel estimation methods [11], [13], [25] require the pilot overhead to be linearly dependent on N, while our IRF method needs exactly 3 pilot slots, regardless of the number of RIS elements.

The computational complexity of processing the obtained power signals depends on the hardware implementation. The $\mathcal{O}(1)$ time complexity only holds when one MCU is installed for each RIS element. If all the RIS elements are collectively controlled by one processor, the computational time would be $\mathcal{O}(N)$, but the pilot overhead still remains $\mathcal{O}(1)$. These conclusions of complexity can be easily extended to multi-RIS schemes, where multiple RISs are employed to serve a single user at the same time. The independent nature of IRF methods allows the RISs

to work without the need to exchange data with the BS or other RISs. This property makes it much easier to integrate a new RIS into an existing communication system, which greatly enhances the extendibility of the system.

V. Phase Estimation Algorithms

In this section, three phase estimation algorithms will be proposed in Subsection V-A, V-B, and V-C respectively, which constitute the core of the IRF channel estimation and beamforming algorithm.

A. DFT method

The key challenge of the IRF channel estimation and beamforming is the phase estimation step, i.e., how to obtain the phase difference φ. Since the interferential power $P(t)$ exhibits a sinusoidal waveform, Fourier transforms can be applied to extract its phase. Apply L-point discrete Fourier transform (DFT) to the discrete-time observed sensor detection signals $P[0], \cdots, P[L-1]$, and we have

$$p[l'] = \sum\nolimits_{l=0}^{L-1} P[l] e^{-\mathrm{j}\frac{2\pi}{L} l l'}, \quad \forall l' \in \{L\}. \tag{11}$$

Specifically, we have the complex amplitude of the first harmonic $p[1]$ as

$$p[1] = \sum\nolimits_{l=0}^{L-1} A \left[\alpha^2 + \beta^2 + 2\alpha\beta \cos\left(\frac{2\pi}{L} l + \varphi\right)\right] e^{-\mathrm{j}\frac{2\pi}{L} l} = LA\alpha\beta e^{\mathrm{j}\varphi}. \tag{12}$$

Then, the phase φ can be estimated as

$$\hat{\varphi} = \arg\left(\frac{p[1]}{LA\alpha\beta}\right) = \arg\left(p[1]\right). \tag{13}$$

Note that this DFT method simply ignores the non-Gaussian noise. For Gaussian noise, the DFT method is optimal. However, in fact, the noise in (10) contains a squared term of Gaussian noise, resulting in the noise being non-Gaussian. Thus, we further conceive an ML method, as described in the following Subsection V-B.

B. Newton-ML method

Suppose the noise field $v'(t) = v'_R(t) + \mathrm{j}v'_I(t) \sim \mathcal{CN}(0, \sigma_v^2)$, and the noise of the power sensor is $\zeta \sim \mathcal{N}(0, \sigma_\zeta^2)$. Without loss of generality, we can assume that the sensor noise power σ_ζ^2 is much weaker than the electromagnetic noise field $v'(t)$. Thus, we assume $\sigma_\zeta^2 = 0$ in the following

discussion. As a result, the distribution of $P(t) = A\left|E_{\mathrm{BB,IRF}}(t)\right|^2$ is a non-central chi-squared distribution $\mathcal{NC}_{\chi_2^2}(A(\mu_R^2+\mu_I^2), A\sigma_v^2/2)$ with degrees of freedom $k=2$, and mean values μ_R, μ_I given by

$$\mu_R = \alpha + \beta\cos(\psi(t)+\varphi), \quad \mu_I = \beta\sin(\psi(t)+\varphi). \tag{14}$$

Thus, according to (10), the output signal of the power sensor is given by

$$P(t) = A\left((v_R'+\mu_R)^2 + (v_I'+\mu_I)^2\right) \tag{15}$$

Let us define the noncentral parameter $\lambda(t)$ as

$$\lambda(t) = A(\mu_R^2+\mu_I^2) = A\left[\alpha^2+\beta^2+2\alpha\beta\cos\left(\psi(t)+\varphi\right)\right], \tag{16}$$

then, according to the definition of the $\mathcal{NC}_{\chi_2^2}$, the p.d.f of $P(t)$ is given by the zeroth-order modified Bessel function of the first kind

$$f_P(x) = \frac{1}{A\sigma_v^2}\exp\left(-\frac{x+\lambda(t)}{A\sigma_v^2}\right) I_0\left(\frac{\sqrt{\lambda(t)x}}{A\sigma_v^2/2}\right), \quad x \geq 0. \tag{17}$$

Then, the log likelihood function of φ based on the observations $P[l]$ can be represented by

$$\mathcal{L}(P[0],\cdots,P[L-1]|\varphi) = \sum_{l=0}^{L-1}\left[-\frac{P[l]+\lambda_l}{A\sigma_v^2} + \log I_0\left(\frac{\sqrt{P[l]\lambda_l}}{A\sigma_v^2/2}\right)\right] - L\log(A\sigma_v^2), \tag{18}$$

where $\lambda_l := \lambda(t_l)$, and the derivative of (18) is

$$\frac{\partial\mathcal{L}(P[0],\cdots,P[L-1]|\varphi)}{\partial\varphi} = \frac{2\alpha\beta}{\sigma_v^2}\sum_{l=0}^{L-1}\sin(\psi(t_l)+\varphi)\left[1 - R\left(\frac{\sqrt{P[l]\lambda_l}}{A\sigma_v^2/2}\right)\frac{\sqrt{P[l]}}{\sqrt{\lambda_l}}\right], \tag{19}$$

where the function $R(z)$ is defined as $R(z) = I_1(z)/I_0(z)$. Since the derivative of the function $R(z)$ satisfies the property [26]

$$R'(z) = 1 - R^2(z) - \frac{1}{z}R(z), \tag{20}$$

the second derivative of the likelihood function $\mathcal{L}$ can be expressed as

$$\begin{aligned}\frac{\partial^2\mathcal{L}(P[0],\cdots,P[L-1]|\varphi)}{\partial\varphi^2} =&\frac{2\alpha\beta}{\sigma_v^2}\sum_{l=0}^{L-1}\cos(\psi(t_l)+\varphi)\left[1-R\left(z_l\right)\frac{\sqrt{P[l]}}{\sqrt{\lambda_l}}\right]\\ &+\frac{4\alpha^2\beta^2}{\sigma_v^4}\sum_{l=0}^{L-1}\sin^2(\psi(t_l)+\varphi)\left(1-R^2(z_l)-\frac{2}{z_l}R(z_l)\right)\frac{P[l]}{\lambda_l},\end{aligned} \tag{21}$$

where $z_l=\sqrt{P[l]\lambda(t_l)}/(A\sigma_v^2/2)$. Then, we can perform the Newton iteration to obtain $\hat{\varphi}$, by iteratively using the updating formula

$$\hat{\varphi}^{(k+1)}=\hat{\varphi}^{(k)}-\frac{\mathcal{L}'(\hat{\varphi}^{(k)})}{\mathcal{L}''(\hat{\varphi}^{(k)})}, \tag{22}$$

where $\mathcal{L}'(\hat{\varphi}^{(k)})$ and $\mathcal{L}''(\hat{\varphi}^{(k)})$ are given by (19) and (21) respectively. Note that during the calculation of (22), A,σ_v,α,β and the received signal $P[l]$ are all assumed to be known. Thus, in fact, (19) and (21) are functions of a single variable φ.

C. von Mises-EM method

The Newton-ML algorithm, if convergent, is asymptotically optimal [27]. However, the computation of the Newton-ML estimator is quite complicated due to the intensive calculation of modified Bessel functions. Now we introduce an iterative method for estimating φ without any computation of such special functions. Our method is based on the von Mises distributions [28].

The von Mises-EM algorithm is based on the Bayesian inference of von Mises distributions [29]. The von Mises distribution $\mathcal{VM}(\mu,\kappa)$ is a two-parameter distribution on $[0,2\pi]$, with the probability density function given by

$$p(\theta|\mu,\kappa)=\frac{\exp(\kappa\cos(\theta-\mu))}{2\pi I_0(\kappa)},\quad 0\le\theta\le 2\pi, \tag{23}$$

where $\mu\in[0,2\pi]$ and $\kappa>0$ being the cyclic location parameter and the concentration parameter. Note that the von Mises distribution is a distribution on a circle, thus it acts as a perfect prior distribution of a phase estimation problem. More fortunately, the von Mises distribution is also closely related to the complex Gaussian distribution, thus implying the possibility of designing an iterative EM algorithm [27] based on the interactions between the von Mises distribution and the complex Gaussian noise distribution. The following two lemmas: **Lemma 1** and **Lemma 2** reveal these interactions.

Lemma 1 (Bayesian estimation of von Mises distribution)

Let $\theta \sim \mathcal{VM}(\mu, \kappa)$, and $z|\theta \sim \mathcal{CN}(e^{\mathrm{j}\theta}, \sigma^2)$. Then the posterior distribution $\theta|z$ is also a von Mises distribution $\mathcal{VM}(\mu', \kappa')$ with parameters μ' and κ' satisfying $\kappa' e^{\mathrm{j}\mu'} = \kappa e^{\mathrm{j}\mu} + 2z/\sigma^2$.

Proof: See **Appendix A**. ■

In this paper, we also use $\mathcal{VM}(\kappa e^{\mathrm{j}\mu})$ to denote the von Mises distribution $\mathcal{VM}(\mu, \kappa)$. This representation provides convenience for the calculation of the posterior distribution of the von Mises distribution in Bayesian inference.

Lemma 2 (Noncentral $\mathcal{CN}$ posterior distribution on circle is $\mathcal{VM}$)

Suppose $z \sim \mathcal{CN}(z_0, \sigma^2)$, where $z_0 \in \mathbb{C}$, and a positive radius $r > 0$. Then the posterior distribution of angle $\theta = \arg(z)$, constrained on a circle $|z| = r$ obeys the von Mises distribution

$$p(\theta|\,|z| = r) \sim \mathcal{VM}\left(\arg(z_0), \frac{r|z_0|}{\sigma^2/2}\right). \tag{24}$$

Proof: Replacing z by $re^{\mathrm{j}\theta}$ give rise to the conclusion immediately. ■

Combining the results of **Lemma 1** and **Lemma 2**, we can then construct the EM algorithm for estimating φ. Since the output of the power sensors $P[l]$ does not contain phase information, we can treat the phases as latent variables. Let $s_l = \sqrt{P[l]/A}$ be the noisy estimation for $|\alpha + \beta e^{\mathrm{j}(\varphi+\psi_l)} + v_l|$, and θ_l be the latent variables $\arg(\alpha + \beta e^{\mathrm{j}(\varphi+\psi_l)} + v_l)$ that are not observable. Since the noise $v_l \sim \text{i.i.d. } \mathcal{CN}(0, \sigma_v^2)$, then from **Lemma 2**, $\theta_l|s_l, \varphi \sim \mathcal{VM}(\arg(\alpha + \beta e^{\mathrm{j}(\varphi+\psi_l)}), s_l|\alpha + \beta e^{\mathrm{j}(\varphi+\psi_l)}|/(\sigma_v^2/2))$. Thus, we can infer the latent variables by ML estimation

$$\hat{\theta}_{l,\mathrm{ML}}|s_l, \varphi = \arg(\alpha + \beta e^{\mathrm{j}(\varphi+\psi_l)}). \tag{25}$$

After inferring the latent variables $\hat{\theta}_{l,\mathrm{ML}}$, we can update the estimation of φ using Bayesian rule in **Lemma 1**

$$\varphi|s_l, \theta_l \sim \mathcal{VM}\left(\kappa e^{\mathrm{j}\mu} + \frac{\beta}{\sigma_v^2/2}\sum_{l=0}^{L-1}\left(s_l e^{\mathrm{j}\theta_l} - \alpha\right)e^{-\mathrm{j}\psi_l}\right), \tag{26}$$

where the coefficient $\beta/(\sigma_v^2/2)$ comes from scaling the phasor in Fig. 3 by a factor β^{-1} and applying **Lemma 1**. Performing E-step with (25) and M-step with (26) alternately, then the estimation precision for φ can be iteratively improved. Note that although the modified Bessel functions appear in the density function of von Mises distribution, the bother is avoided in the von Mises-EM algorithm. The pseudo code of von Mises-EM algorithm is collected in **Algorithm 2**.

Algorithm 2 von Mises-EM phase estimation (VM-EM algorithm)

Input: Incident wave intensity α, β; sensor data $P[l]$; amplification factor A and noise variance σ_v^2; predefined phase shifts $\psi_l = \omega t_l$.

Output: $\hat{\varphi}$

$s_l \leftarrow \sqrt{P[l]/A}, \quad \forall l \in \{L\}$
$\hat{\varphi} \leftarrow \arg\{\mathrm{FFT}(P)[1]\}$
$\kappa \leftarrow 1$
while $\hat{\varphi}$ not convergence **do**
  $\mu_l \leftarrow \alpha + \beta e^{\mathrm{j}(\hat{\varphi}+\psi_l)}, \quad \forall l \in \{L\}$
  $w_l \leftarrow s_l e^{\mathrm{j}\arg(\mu_l)} - \alpha, \quad \forall l \in \{L\}$
  $z_\varphi \leftarrow \kappa e^{\mathrm{j}\hat{\varphi}} + \beta \left(\sum_{l=0}^{L-1} w_l e^{-\mathrm{j}\psi_l} \right) / (\sigma_v^2/2)$
  $\hat{\varphi} \leftarrow \arg(z_\varphi)$
  $\kappa \leftarrow |z_\varphi|$
end while
return $\hat{\varphi}$

VI. Performance Analysis

In this section, we derive the exact expression of the CRLB in the phase estimation problem. To simplify the calculation, we provide an asymptotic expression of the CRLB. Moreover, we also reveal the mathematical properties of the obtained CRLB and provide the error analysis.

A. Exact Expression of the CRLB

In Section IV, we have introduced three phase estimation methods to solve the probabilistic parameter estimation problem. We derive the CRLB [27] of the estimation in **Theorem 1**.

Theorem 1 (Non-central Chi-Squared CRLB)

Suppose the probabilistic model is specified by (15)*, where L observations $P[0], \cdots, P[L-1]$ are obtained. Then the CRLB of this L-point phase estimation problem is given by*

$$\frac{1}{\mathrm{CRLB}(\varphi)} = K^2(\bar{\gamma})^2 \sum_{l=0}^{L-1} \sin^2(\psi_l + \varphi) \left(1/\gamma_l - g(\gamma_l)\right), \tag{27}$$

where $K = 2\alpha\beta/(\alpha^2+\beta^2)$, $a = A\sigma_v^2$, $\gamma_l = \lambda_l/a = \left(\alpha^2+\beta^2+2\alpha\beta\cos(\psi_l+\varphi)\right)/\sigma_v^2$, and $\bar{\gamma}$ is

the arithmetic mean of all the $\gamma_0, \cdots, \gamma_{L-1}$. *The function* $g(\gamma)$ *is defined as*

$$g(\gamma) = \int_0^{+\infty} \gamma t \exp(-\gamma(1+t))\, I_0\left(2\gamma\sqrt{t}\right)\, \left(1 - R^2\left(2\gamma\sqrt{t}\right)\right) \mathrm{d}t. \tag{28}$$

Proof: See **Appendix B**. ■

From **Theorem 1**, we note that the CRLB of the phase estimation problem is completely determined by the two parameters K and $\bar{\gamma}$, which are the interferential contrast and the average interferential SNR, respectively. However, this exact CRLB expression is difficult to calculate due to the sophisticated evaluation of the integral in (28). Thus, we will provide a simpler approximated CRLB in the following Subsection VI-B.

B. Asymptotic CRLB

Theorem 2 (Asymptotic Evaluation of Noncentral Chi-Squared CRLB)

Suppose the probabilistic model is specified by (15). *Then the approximated CRLB of this* L*-point phase estimation problem is given by*

$$\frac{1}{\mathrm{CRLB}(\varphi)} \approx K^2(\bar{\gamma})^2 \sum_{l=0}^{L-1} \sin^2(\psi_l + \varphi)(1/\gamma_l - \hat{g}(\gamma_l))^+, \tag{29}$$

where $(x)^+$ *represents* $x\mathbb{1}_{\{x\geq 0\}}$, *and the definition of parameters are the same as in* **Theorem 1**. *The asymptotic approximation function* $\hat{g}(\gamma)$ *is defined as*

$$\hat{g}(\gamma) = \frac{1}{4}\sqrt{\frac{\pi}{\gamma}} e^{-\gamma/2} \left((1+1/\gamma) I_0(\gamma/2) + I_1(\gamma/2)\right). \tag{30}$$

Proof: See **Appendix C**. ■

The asymptotic expression of the CRLB still relies only on two parameters K and $\bar{\gamma}$. But the calculation is much simpler compared to the exact expression. The discussions of the properties of the exact and asymptotic expressions of CRLB are continued in Subsection VI-C.

C. Properties of the CRLB

From the above analysis of CRLB, we can observe two properties of the phase estimation problem:

1) The CRLB relies almost only on the physical parameters K and $\bar{\gamma}$.
2) The CRLB is insensitive to the value φ.

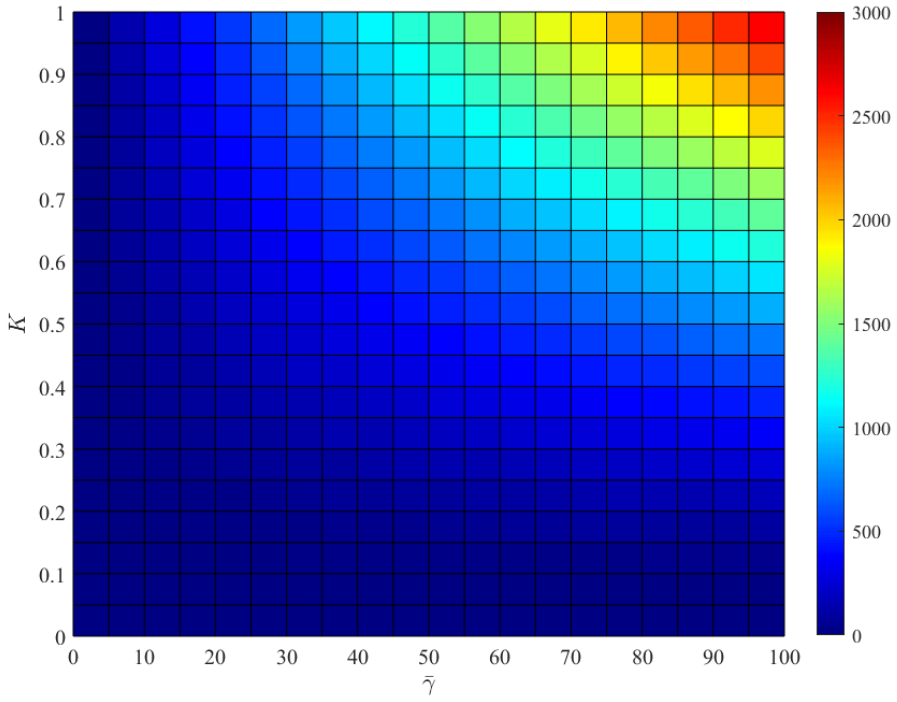

Fig. 5. Precise $1/\mathrm{CRLB}(\varphi)$ as a two-variable function of K and $\bar{\gamma}$, calculated from (27). The larger the value of the reciprocal CRLB, the more precise an unbiased estimator can be.

The first point can be concluded from the expressions, and the second point comes from the symmetry of the $\sin^2(\cdot)$ function when L is large enough. We have plotted $1/\mathrm{CRLB}(\varphi)$ as a two-variable function in Fig. 5. The best prediction accuracy occurs when $|K| = 1$, i.e., the RIS-received signal from BS is as strong as that from the user. Also, the larger value of the average interferential SNR $\bar{\gamma}$ also contributes to a more accurate phase estimation.

We also perform error analysis for the use of asymptotic expansion technique, which is stated in the following **Theorem 3**.

Theorem 3 (CRLB Approximation by Asymptotic Expansion is Asymptotically Optimal) *The relative error r of $1/\gamma - \hat{g}(\gamma)$, as an approximation of $1/\gamma - g(\gamma)$, decreases at a rate that is inverse proportional to the interferential SNR γ, i.e.,*

$$r = \frac{|\hat{g}(\gamma) - g(\gamma)|}{1/\gamma - g(\gamma)} = \mathcal{O}\left(\frac{1}{\gamma}\right). \tag{31}$$

Proof: See **Appendix D**. ■

From **Theorem 3**, we can conclude that our derived expression of approximated CRLB is asymptotically optimal.

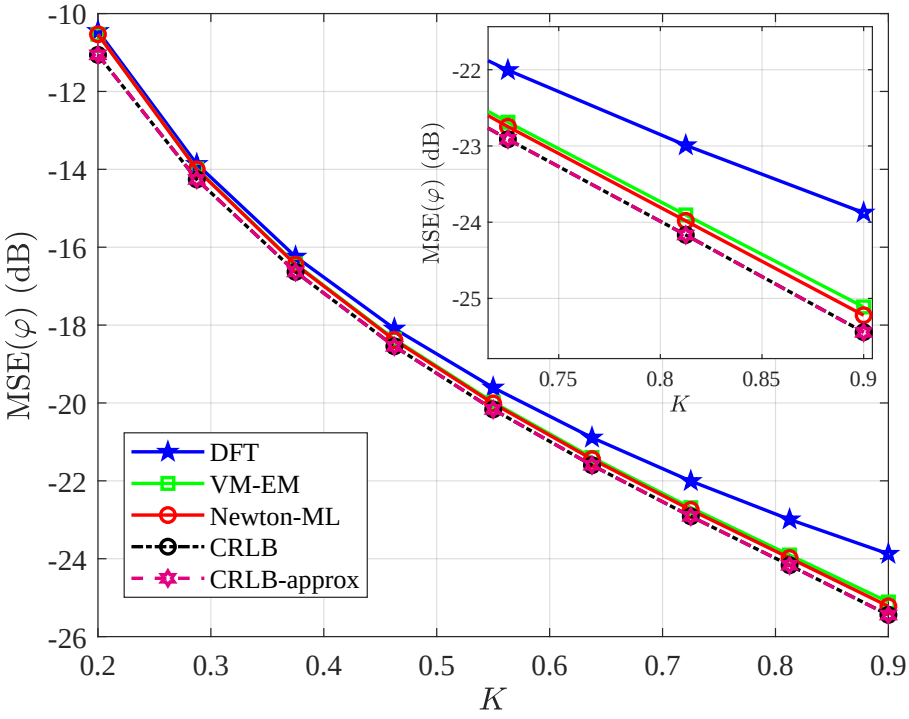

Fig. 6. Performance comparison of phase estimation algorithms. x-axis represents the interferential contrast K; y-axis represents the MSE of the estimators. The VM-EM algorithm outperforms naive DFT by at least $1\,\mathrm{dB}$ in high-K regions.

VII. Simulation Results

In this section, we will present our simulation results. In Subsection VII-A, we will show the performance comparison of the phase estimation algorithms. In Subsection VII-B, we will show the achievable rate comparison of our IRF method and other RIS-aided channel estimation and beamforming algorithms.

A. Phase Estimation Algorithms

In Section IV, we have already introduced three phase estimation algorithms: DFT, Newton-ML and VM-EM. Now we compare the performance of these algorithms together with the CRLB which has been derived in Section VI. In all the simulations for phase estimation algorithms, the amplification factor A is fixed to be 1, the number of power samples[5] is fixed to $L = 2^6 = 64$, and $\sigma_\zeta = 0.05$; The interferential SNR $\bar{\gamma} = 20$ in Fig. 6. The CRLB and CRLB-approx curves

[5]In practical OFDM systems, the number of signal samples within the duration of an OFDM symbol is usually ~ 2048. Considering that the power sensor is usually slower than the baseband ADC, it is reasonable to assume a 32-times slower sampling rate of the power sensor. Thus, $L = 64$ is a reasonable number of acquired power samples during one time slot.

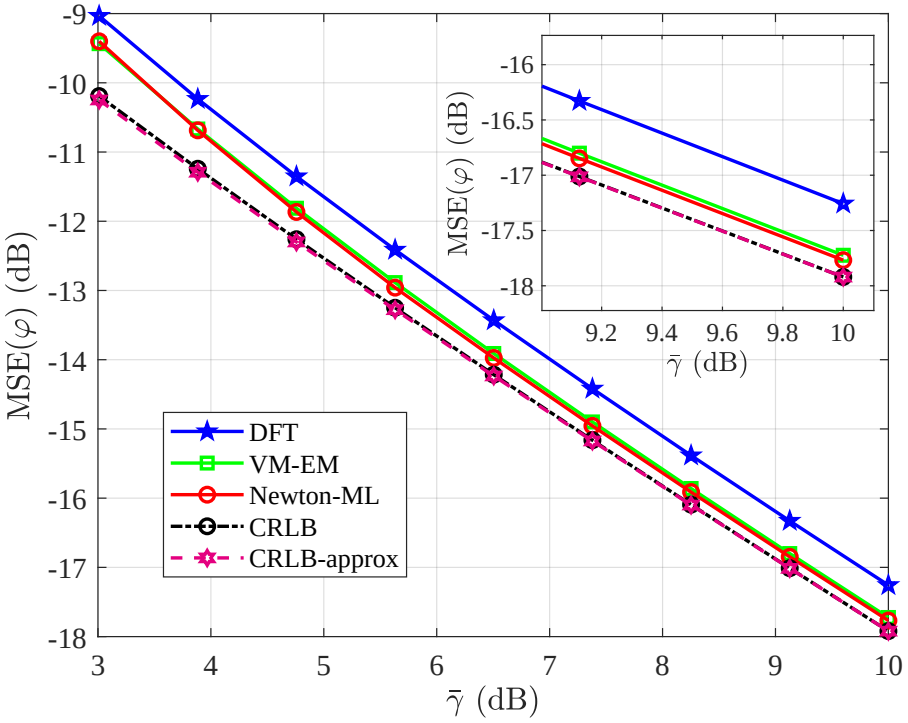

Fig. 7. Performance comparison of phase estimation algorithms. x-axis represents the average interferential SNR $\bar{\gamma}$; y-axis represents the MSE of the estimators. The interferential contrast $K = 0.6$.

are calculated from (27) and (29), respectively. For Newton-ML algorithm, the Newton iteration is performed 4 times according to (22). For VM-EM algorithm, the iteration number is also fixed to 4. The true value of random variable φ under estimation is drawn from a uniform distribution on $[0, 2\pi]$. In the simulations in Fig. 7, all the simulation parameters, except for K and $\bar{\gamma}$, are the same with Fig. 6.

From Fig. 6 and Fig. 7 we discover that the VM-EM algorithm has comparable performance with the Newton-ML algorithm, but the computational cost is significantly lower, since **Algorithm 2** does not require the evaluation of the complicated modified Bessel functions. Both the Newton-ML and VM-EM algorithms are close to the CRLB, and both of them outperform the simple DFT algorithm[6]. The CRLB approximation is also satisfactory under a wide range of K and $\bar{\gamma}$.

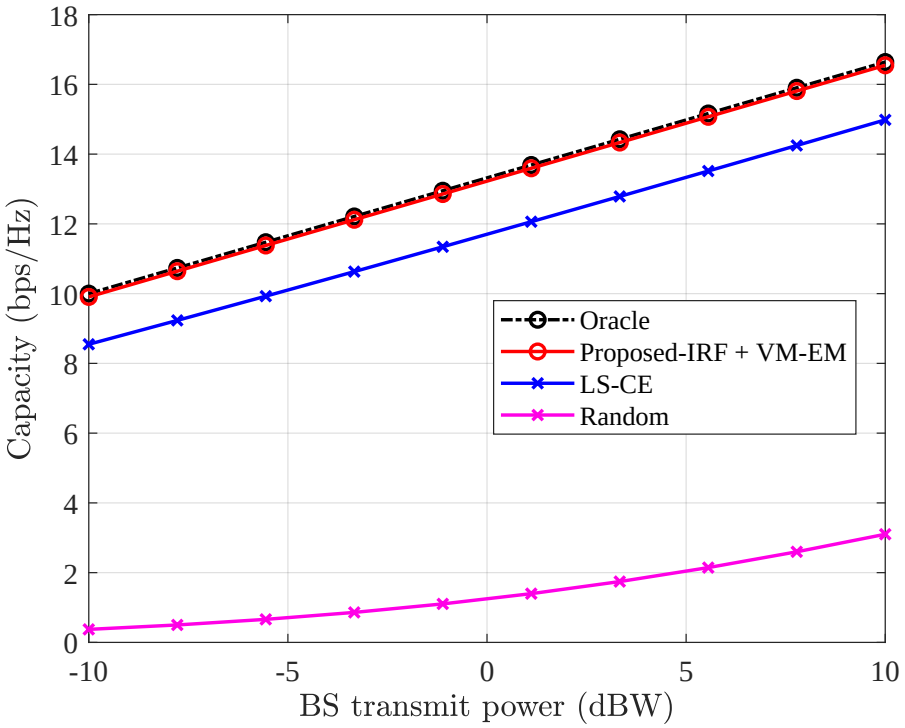

Fig. 8. Performance curve of the achievable spectral efficiency against the BS transmitted power $P_{\max}$.

B. Achievable Spectral Efficiency under IRF

All our simulation data are acquired under $f_c = 10\,\mathrm{GHz}$, $P'_{\max} = 300\,\mathrm{mW}$, $n_0 = -174\,\mathrm{dBm/Hz}$, subcarrier bandwidth $\mathrm{BW} = 180\,\mathrm{kHz}$, thermal noise at the receiver $\sigma^2 = \mathrm{BW} \times n_0$, $\sigma_v^2 = 100\,\mathrm{MHz} \times n_0 F_p$, where $F_p = 10\,\mathrm{dB}$ is the noise factor of the power sensor, and the BS-RIS and RIS-user channels are all assumed to be Rayleigh fading with 1 line-of-sight (LOS) path and 4 none-line-of-sight (NLOS) paths. The Rician κ-factor is $\kappa = 2$. Both the BS and the RIS are equipped with $\lambda/2$-spaced uniform planar arrays (UPAs), while the user has a single antenna. The BS is located at a distance from the RIS that is drawn from a uniform distribution between $20\,\mathrm{m}$ and $100\,\mathrm{m}$, and the angle of the BS is uniformly distributed. The user appears uniformly from $10\,\mathrm{m}$ to $100\,\mathrm{m}$, and the angle distribution of the user is also uniform. The size of the RIS is set to be 40×30, and that of the BS antenna is 4×2. For IRF methods, 3 pilots are used for CSI acquisition. However, for LS-CE methods, the number of pilots is $N = 40 \times 30$.

We compare our proposed IRF channel estimation and beamforming method with classical

[6]The DFT estimator in Fig. 7 exhibits a near-constant performance gap toward the CRLB in the high-SNR region, while the Newton-ML and VM-EM estimators seem to bridge this gap and finally approaches the CRLB as $\bar{\gamma} \to \infty$.

LS-CE algorithm and other idealized settings in Fig. 8. In the simulation of our IRF method, the VM-EM phase estimation algorithm is utilized with the assumption that the phases of the BS-RIS LOS path are known. The black dashed line "Oracle" assumes perfectly-known CSI, thus perfect iterative beamforming can be performed. In the LS-CE method, we first utilize (7) to obtain estimates for the cascaded channel [5], [14], and then perform iterative RIS beamforming based on the estimated channel. In addition, we also consider the randomly-phased RIS scheme as a benchmark.

Fig. 8 shows the performance curve of the achievable spectral efficiency against the BS transmitted power. From this figure, we can conclude that the proposed IRF method with VM-EM phase estimation is nearly optimal, under extremely low pilot overhead. The proposed IRF method is even close to the oracle scheme, and achieves satisfactory performance throughout a wide range of the BS transmitted power.

VIII. Conclusion

In this paper, we have introduced a dimension-independent CSI acquisition method for sensing RIS-assisted MISO wireless communication systems. Combined with our proposed VM-EM phase estimation algorithm, the pilot overhead of our CSI acquisition method is made independent of the number of RIS elements with low computational cost, enabling the implementation of extremely large-scale RISs to achieve significant beamforming gain. Both CRLB analysis and simulation results verified the near-optimality of our VM-EM algorithm. Furthermore, due to the independent property of our IRF-based CSI acquisition method, the near-field effect cannot corrupt the precision of the CSI. Also due to the simultaneous signaling protocol, the "multiplicative fading" effect of RIS [30], [31] during channel estimation is automatically avoided. Thus, the IRF method has a promising future in high-frequency large-scale systems.

For future work, the spatial interferential fringes on the sensing RIS may be exploited to recover the CSI at higher precision, and the data obtained by the power sensors may be utilized to perform joint channel estimation and beamforming together with traditional methods. In addition, different interferential frequencies can be assigned to different users to perform multi-user CSI acquisition within a single time slot, but the waveforms should be re-designed to avoid interference among users. Furthermore, when equipped with a sensing RIS, traditional MIMO systems can also benefit from the additional CSI provided by the phase estimation methods based on the IRF.

APPENDIX A
PROOF OF **LEMMA 1**

Denote $z = z_r + \mathrm{j}z_i$; then the posterior density $p(\theta|z) \propto p(\theta)p(z|\theta)$ can be expressed as

$$\begin{aligned} p(\theta|z) &\propto \exp(\kappa\cos(\theta-\mu))\exp\left(-\frac{1}{\sigma^2}\left((z_r-\cos\theta)^2+(z_i-\sin\theta)^2\right)\right) \\ &\propto \exp\left(\kappa\cos(\theta-\mu)+\frac{2}{\sigma^2}(z_r\cos\theta+z_i\sin\theta)\right) \\ &\propto \exp\left(\mathrm{Re}\left[e^{\mathrm{j}\theta}\left(\kappa e^{-\mathrm{j}\mu}+\frac{1}{\sigma^2/2}z^*\right)\right]\right). \end{aligned} \tag{32}$$

Since the density of the von Mises distribution $\mathcal{VM}(\mu,\kappa)$ can also be expressed as $p(\theta) \propto \exp\left(\mathrm{Re}\left[e^{\mathrm{j}\theta}(\kappa e^{\mathrm{j}\mu})^*\right]\right)$, we can also parameterize the von Mises distribution by a single complex parameter $\kappa e^{\mathrm{j}\mu}$. Thus, the above $p(\theta|z)$ is a von Mises density with parameter $\kappa' e^{\mathrm{j}\mu'}$, satisfying $\kappa' e^{\mathrm{j}\mu'} = \kappa e^{\mathrm{j}\mu} + 2z/\sigma^2$. This completes the proof.

APPENDIX B
PROOF OF **THEOREM 1**

According to the definition of the CRLB, taking the negative expectation of (21) yields the reciprocal CRLB of the estimators for φ. Note that in (21), there are three types of expectations to be evaluated: $\mathbb{E}\left[P[l]\right]$, $\mathbb{E}\left[R(z_l)\sqrt{P[l]}\right]$, and $\mathbb{E}\left[(1-R^2(z_l))P[l]\right]$. The expectation of $P[l]$ can be directly evaluated from (15) by the linearity of the expectation operation:

$$\mathbb{E}\left[P[l]\right] = A\sigma_v^2 + \lambda_l. \tag{33}$$

The expectation $\mathbb{E}\left[R(z_l)\sqrt{P[l]}\right]$ can be evaluated by calculating the derivative w.r.t λ_l on both sides of the identity $\mathbb{E}_{\lambda_l, A\sigma_v^2}[e^{\lambda_l/(A\sigma_v^2)}] = e^{\lambda_l/(A\sigma_v^2)}$:

$$\begin{aligned} \mathbb{E}\left[R(z_l)\sqrt{P[l]}\right] &= e^{-\lambda_l/(A\sigma_v^2)}\int_0^{+\infty}\frac{1}{A\sigma_v^2}\exp\left(-\frac{x}{A\sigma_v^2}\right)I_1\left(\frac{\sqrt{\lambda_l x}}{A\sigma_v^2/2}\right)\sqrt{x}\mathrm{d}x \\ &= e^{-\lambda_l/(A\sigma_v^2)}A\sigma_v^2\sqrt{\lambda_l}\frac{\partial}{\partial\lambda_l}\int_0^{+\infty}\frac{1}{A\sigma_v^2}\exp\left(-\frac{x}{A\sigma_v^2}\right)I_0\left(\frac{\sqrt{\lambda_l x}}{A\sigma_v^2/2}\right)\mathrm{d}x \\ &= \sqrt{\lambda_l}. \end{aligned} \tag{34}$$

According to the definition of z_l, the expectation $\mathbb{E}\left[R(z_l)P[l]/z_l\right]$ is of the same form as the expectation $\mathbb{E}\left[R(z_l)\sqrt{P[l]}\right]$. Thus, the expectation result is

$$\mathbb{E}\left[\frac{R(z_l)}{z_l}P[l]\right] = \frac{A\sigma_v^2}{2}. \tag{35}$$

As for the third kind of expectation $\mathbb{E}\left[(1-R^2(z_l))\frac{P[l]}{\lambda_l}\right]$, we first define

$$g(\lambda_l, a) = \mathbb{E}\left[(1-R^2(z_l))\frac{P[l]}{\lambda_l}\right]. \tag{36}$$

Let $x = \lambda_l t$, and write down the integral expression of (36), we obtain

$$\begin{aligned} g(\lambda_l, a) &= \int_0^{+\infty} t(1-R^2(2\gamma_l\sqrt{t}))\frac{\lambda_l}{a}\exp\left(\frac{\lambda_l+\lambda_l t}{a}\right) I_0\left(2\gamma_l\sqrt{t}\right)\mathrm{d}t \\ &= \int_0^{+\infty} \gamma_l t\exp(-\gamma_l(1+t))\, I_0\left(2\gamma_l\sqrt{t}\right)\,\left(1-R^2\left(2\gamma_l\sqrt{t}\right)\right)\mathrm{d}t \\ &= g(\gamma_l). \end{aligned} \tag{37}$$

Combining the above equations of expectations (33), (34), (35) and (37), we obtain

$$\begin{aligned} \frac{1}{\mathrm{CRLB}(\varphi)} &\overset{(a)}{=} -\frac{4\alpha^2\beta^2}{\sigma_v^4}\sum_{l=0}^{L-1}\sin^2(\psi(t_l)+\varphi)\left(\mathbb{E}\left[(1-R^2(z_l))\frac{P[l]}{\lambda_l}\right]-\frac{a}{\lambda_l}\right) \\ &\overset{(b)}{=} \frac{4\alpha^2\beta^2}{\sigma_v^4}\sum_{l=0}^{L-1}\sin^2(\psi(t_l)+\varphi)\left(\frac{a}{\lambda_l}-g(\lambda_l/a)\right), \end{aligned} \tag{38}$$

where step (a) comes from substituting these three types of expectation into (21), and step (b) comes from replacing the trickiest expectation by the definition of the function $g(\cdot)$ in (28).

Note that the precise value of the CRLB can be determined by the exact single-variable g function (28), whose variable $\gamma_l = \lambda_l/a$ is the interferential SNR. After further derivations, it can be observed from the expressions that the CRLB only relies on two intrinsic physical parameters: the interferential SNR γ_l, and the interferential contrast K [20], which coincides with the physical intuition. Imitating the notations in optics, we define the parameter K to be

$$K = \frac{I_M - I_m}{I_M + I_m} = \frac{2\alpha\beta}{\alpha^2+\beta^2}, \tag{39}$$

and K automatically satisfies $-1 \le K \le 1$. Define the average interferential SNR $\bar{\gamma}$ to be the

arithmetic average of $\gamma_l, 0 \leq l < L$:

$$\bar{\gamma} = \frac{1}{L}\sum_{l=0}^{L-1}\gamma_l = \frac{\alpha^2+\beta^2}{\sigma_v^2}. \tag{40}$$

Thus, the CRLB can be expressed as

$$\frac{1}{\mathrm{CRLB}(\varphi)} = K^2(\bar{\gamma})^2\sum_{l=0}^{L-1}\sin^2(\psi_l+\varphi)\left(1/\gamma_l - g(\gamma_l)\right) \tag{41}$$

where the values $\gamma_l = \bar{\gamma}\left(1+K\cos(\psi_l+\varphi)\right)$ are jointly determined by both the average interferential SNR $\bar{\gamma}$ and the interferential contrast K. This completes the proof.

APPENDIX C
PROOF OF **THEOREM 2**

Since an exact expression of $g(\gamma)$ in (28) is difficult to calculate, we evaluate it approximately by utilizing the asymptotic expansion $x(1-R^2(2\sqrt{x})) \approx \sqrt{x}/2$ [26]. According to the definition, evaluating $g(\gamma)$ is the same as evaluating $\mathbb{E}[(1-R^2(z_l))P[l]/\lambda_l]$.

In order to evaluate the expectation $\mathbb{E}[(1-R^2(z_l))P[l]/\lambda_l]$, we first introduce some preliminaries about the noncentral chi distribution $\mathcal{NC}_{\chi_k}(\lambda)$ with noncentrality parameter $\lambda > 0$. The distribution $\mathcal{NC}_{\chi_k}(\lambda)$ is the law of the length (2-norm) of a k-dimensional standard normal distribution $\mathcal{N}(\boldsymbol{\mu}, \boldsymbol{I}_k)$, with $\lambda = \|\boldsymbol{\mu}\|_2$. Specifically, we are interested in the case where $k=2$, since this is the case of the 2-dimensional complex plane. For $k=2$, let $Y \sim \mathcal{NC}_{\chi_2}(m)$, then we have [32]

$$\mathbb{E}\left[Y\right] = \sqrt{\frac{\pi}{2}}L_{1/2}(-m^2/2), \tag{42}$$

where $L_{1/2}$ denotes the generalized Laguerre function of order $1/2$. The function $L_{1/2}(x)$ has explicit expression

$$L_{1/2}(x) = e^{x/2}\left[(1-x)I_0\left(-\frac{x}{2}\right) - xI_1\left(-\frac{x}{2}\right)\right]. \tag{43}$$

Recall that the asymptotic expansion $x(1-R^2(2\sqrt{x})) \sim \sqrt{x}/2$ holds for large x, and the random variable $P[l]$ obeys a non-central chi-squared distribution which can be equivalently expressed as

$$P[l] \sim A\left|\mathcal{CN}\left((\alpha+\beta e^{\mathrm{j}(\psi_l+\varphi)}), \sigma_v^2\right)\right|^2 \sim \frac{a}{2}\left|\mathcal{CN}\left((\alpha+\beta e^{\mathrm{j}(\psi_l+\varphi)})/(\sigma_v/\sqrt{2}), 2\right)\right|^2. \tag{44}$$

Thus, we obtain

$$\begin{aligned}\mathbb{E}[(1-R^2(z_l))P[l]/\lambda_l] &= \mathbb{E}\left[\left(1-R^2\left(\frac{\sqrt{\lambda_l P[l]}}{a/2}\right)\right)\frac{P[l]}{\lambda_l}\right] \\ &\approx \left(\frac{a}{\lambda_l}\right)^2 \mathbb{E}\left[\sqrt{\frac{\lambda_l P[l]}{a^2}}/2\right] \\ &= \frac{1}{2}\frac{\sqrt{\lambda_l}}{a}\left(\frac{a}{\lambda_l}\right)^2 \sqrt{\frac{a}{2}}\mathbb{E}\left[\mathcal{NC}_{\chi_2}(m)\right],\end{aligned} \tag{45}$$

where $m = |\alpha+\beta e^{\mathrm{j}(\psi_l+\varphi)}|/(\sigma_v/\sqrt{2}) = \sqrt{2\lambda_l/a} = \sqrt{2\gamma_l}$, and thus $m^2/2 = \gamma_l$. Plugging (42) and (43) into (45), we obtain the final expression

$$\begin{aligned}\mathbb{E}[(1-R^2(z_l))P[l]/\lambda_l] &\approx \frac{1}{2}\frac{\sqrt{\lambda_l}}{a}\left(\frac{a}{\lambda_l}\right)^2 \sqrt{\frac{a}{2}}\sqrt{\frac{\pi}{2}}e^{-\gamma_l/2}\left[(1+\gamma_l)I_0(\gamma_l/2)+\gamma_l I_1(\gamma_l/2)\right] \\ &= \frac{1}{4}\sqrt{\frac{\pi}{\gamma_l}}e^{-\gamma_l/2}\left[(1+\gamma_l^{-1})I_0(\gamma_l/2)+I_1(\gamma_l/2)\right] \\ &:= \hat{g}(\gamma_l).\end{aligned} \tag{46}$$

Finally, substituting the approximation (46) into the exact CRLB (27) yields the conclusion (29), which completes the proof. Note that the operation $(x)^+$ in (29) ensures that each term of the CRLB is non-negative.

APPENDIX D
PROOF OF **THEOREM 3**

Since the only imprecise step of the above derivation is the asymptotic expansion, the approximation error of the expectation can be upper-bounded by the asymptotic expansion error. Assume that the asymptotic expansion error does not exceed δ, i.e.,

$$\left|x\left(1-R^2(2\sqrt{x})\right)-\sqrt{x}/2\right| \le \delta. \tag{47}$$

Then, by error analysis on (45), we have

$$|g(\gamma)-\hat{g}(\gamma)| \le \frac{1}{\gamma^2}\delta. \tag{48}$$

It can be numerically confirmed from Fig. 9 that $\delta \le 0.07$, and that as $x \to \infty$, the approximation error tends to zero. Thus, (46) is a nearly perfect approximation when the interferential SNR γ

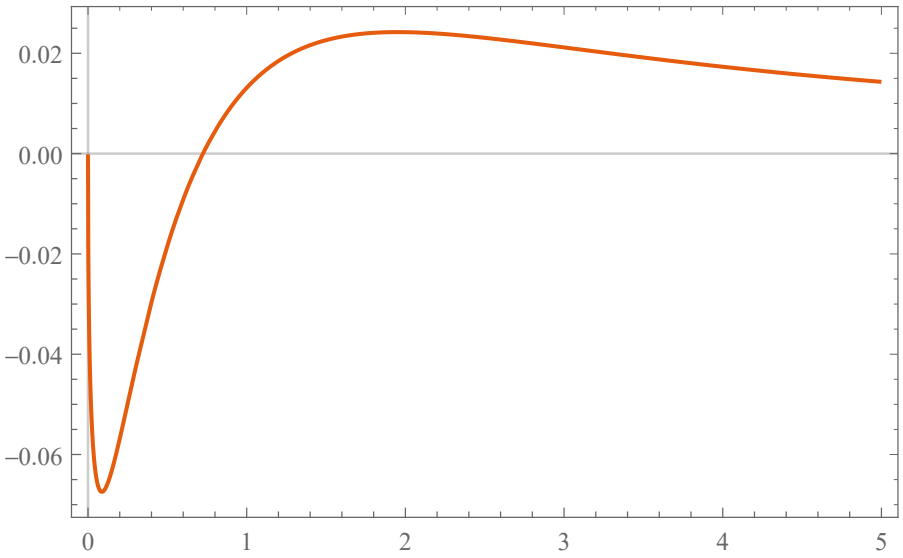

Fig. 9. The curve $x(1-R^2(2\sqrt{x}))-\sqrt{x}/2$, when $0 \leq x \leq 5$. We can see from the curve that the approximation error $\delta \leq 0.07$.

is large. To be more precise, at $\gamma \to +\infty$, the function $\hat{g}(\gamma)$ can be asymptotically expanded as

$$\hat{g}(\gamma) \sim \frac{1}{2}\left(\frac{1}{\gamma}+\frac{1}{4\gamma^2}+\mathcal{O}(\frac{1}{\gamma^3})\right). \tag{49}$$

Thus, $1/\gamma-\hat{g}(\gamma) \sim 1/2\,\Theta(1/\gamma)$, and the relative error r of a single term in the CRLB expression is upper bounded by introducing a positive parameter ϵ, which is

$$\begin{aligned} r &\overset{(a)}{\leq} \frac{\delta/\gamma^2}{\big||1/\gamma-\hat{g}(\gamma)|-|\hat{g}(\gamma)-g(\gamma)|\big|} \\ &\overset{(b)}{\leq} \frac{\delta/\gamma^2}{1/((2+\epsilon)\gamma)-\delta/\gamma^2} \\ &= \frac{\delta}{\gamma/(2+\epsilon)-\delta}, \end{aligned} \tag{50}$$

where (a) comes from applying the triangle inequality, and (b) comes from assuming sufficiently large γ such that the denominator is positive (note that this can be done due to (49)). In order to let this upper bound hold, it should be satisfied that $\gamma > (2+\epsilon)\delta$, and the parameter ϵ should satisfy

$$\frac{1}{\gamma}-\hat{g}(\gamma) > \frac{1}{(2+\epsilon)\gamma}, \quad \forall \gamma > (2+\epsilon)\delta, \tag{51}$$

which is equivalent to

$$\epsilon > \frac{1}{1-\gamma\hat{g}(\gamma)}-2, \quad \forall \gamma > (2+\epsilon)\delta. \tag{52}$$

Such $\epsilon > 0$ exists. Since the function $1/(1-\gamma\hat{g}(\gamma))$ is decreasing for sufficiently large γ, the inequality (52) is equivalent to

$$\epsilon > \frac{1}{1-(2+\epsilon)\delta\,\hat{g}((2+\epsilon)\delta)} - 2. \tag{53}$$

In fact, choosing $\epsilon = 4$ will satisfy all the conditions above when $\delta = 0.07$. Thus, from (50), the relative error is upper bounded by

$$r \leq \frac{0.07}{\gamma/6 - 0.07}, \quad \forall \gamma > 0.42. \tag{54}$$

We can easily see from the above inequality that this approximation becomes arbitrarily good when $\gamma \to \infty$, and the decreasing rate is of order $\mathcal{O}(1/\gamma)$. This completes the proof.

REFERENCES

[1] E. Basar, M. Di Renzo, J. De Rosny, M. Debbah, M.-S. Alouini, and R. Zhang, "Wireless communications through reconfigurable intelligent surfaces," *IEEE Access*, vol. 7, pp. 116 753–116 773, Aug. 2019.

[2] K. Liu, Z. Zhang, L. Dai, and L. Hanzo, "Compact user-specific reconfigurable intelligent surfaces for uplink transmission," *IEEE Trans. Commun.*, vol. 70, no. 1, pp. 680–692, Jan. 2021.

[3] Q. Wu and R. Zhang, "Intelligent reflecting surface enhanced wireless network via joint active and passive beamforming," *IEEE Trans. Wireless Commun.*, vol. 18, no. 11, pp. 5394–5409, Nov. 2019.

[4] M. Di Renzo, A. Zappone, M. Debbah, M.-S. Alouini, C. Yuen, J. De Rosny, and S. Tretyakov, "Smart radio environments empowered by reconfigurable intelligent surfaces: How it works, state of research, and the road ahead," *IEEE J. Sel. Areas Commun.*, vol. 38, no. 11, pp. 2450–2525, Nov. 2020.

[5] X. Wei, D. Shen, and L. Dai, "Channel estimation for RIS assisted wireless communications–Part I: Fundamentals, solutions, and future opportunities," *IEEE Commun. Lett.*, vol. 25, no. 5, pp. 1398–1402, May 2021.

[6] L. Wei, C. Huang, G. C. Alexandropoulos, C. Yuen, Z. Zhang, and M. Debbah, "Channel estimation for RIS-empowered multi-user MISO wireless communications," *IEEE Trans. Commun.*, vol. 69, no. 6, pp. 4144–4157, Jun. 2021.

[7] A. Taha, M. Alrabeiah, and A. Alkhateeb, "Enabling large intelligent surfaces with compressive sensing and deep learning," *IEEE Access*, vol. 9, pp. 44 304–44 321, Sep. 2021.

[8] G. C. Alexandropoulos and E. Vlachos, "A hardware architecture for reconfigurable intelligent surfaces with minimal active elements for explicit channel estimation," in *Proc. IEEE Int. Conf. on Acoust., Speech and Signal Process. (ICASSP)*, May 2020, pp. 9175–9179.

[9] E. Vlachos, G. C. Alexandropoulos, and J. Thompson, "Wideband MIMO channel estimation for hybrid beamforming millimeter wave systems via random spatial sampling," *IEEE J. Sel. Topics Signal Process.*, vol. 13, no. 5, pp. 1136–1150, 2019.

[10] N. T. Nguyen, Q.-D. Vu, K. Lee, and M. Juntti, "Hybrid relay-reflecting intelligent surface-assisted wireless communication," arXiv preprint arXiv:2103.03900, Mar. 2021.

[11] C. Hu, L. Dai, S. Han, and X. Wang, "Two-timescale channel estimation for reconfigurable intelligent surface aided wireless communications," *IEEE Trans. Commun.*, vol. 69, no. 11, pp. 7736–7747, Nov. 2021.

[12] P. Wang, J. Fang, H. Duan, and H. Li, "Compressed channel estimation for intelligent reflecting surface-assisted millimeter wave systems," *IEEE Signal Process. Lett.*, vol. 27, pp. 905–909, May 2020.

[13] Z. Wang, L. Liu, and S. Cui, "Channel estimation for intelligent reflecting surface assisted multiuser communications: Framework, algorithms, and analysis," *IEEE Trans. Wireless Commun.*, vol. 19, no. 10, pp. 6607–6620, Oct. 2020.

[14] N. K. Kundu and M. R. McKay, "Channel estimation for reconfigurable intelligent surface aided MISO communications: From LMMSE to deep learning solutions," *IEEE Open J. Commun. Soc.*, vol. 2, pp. 471–487, 2021.

[15] X. Pei, H. Yin, L. Tan, L. Cao, Z. Li, K. Wang, K. Zhang, and E. Björnson, "RIS-aided wireless communications: Prototyping, adaptive beamforming, and indoor/outdoor field trials," *IEEE Trans. Commun.*, vol. 69, no. 12, pp. 8627–8640, Dec. 2021.

[16] T. Shan, X. Pan, M. Li, S. Xu, and F. Yang, "Coding programmable metasurfaces based on deep learning techniques," *IEEE J. Emerg. Sel. Topics Circ. Syst.*, vol. 10, no. 1, pp. 114–125, 2020.

[17] F. Yang, S. Xu, X. Pan, X. Yang, J. Luo, M. Wang, Y. Wang, and M. Li, "Reconfigurable reflectarrays and transmitarrays: From antenna designs to system applications," in *Proc. 12th European Conference on Antennas and Propagation (EuCAP 2018)*. IET, 2018, pp. 1–4.

[18] S. Atapattu, R. Fan, P. Dharmawansa, G. Wang, J. Evans, and T. A. Tsiftsis, "Reconfigurable intelligent surface assisted two-way communications: Performance analysis and optimization," *IEEE Trans. Commun.*, vol. 68, no. 10, pp. 6552–6567, Oct. 2020.

[19] M. Najafi, V. Jamali, R. Schober, and H. V. Poor, "Physics-based modeling and scalable optimization of large intelligent reflecting surfaces," *IEEE Trans. Commun.*, vol. 69, no. 4, pp. 2673–2691, Apr. 2020.

[20] F. Louradour, F. Reynaud, B. Colombeau, and C. Froehly, "Interference fringes between two separate lasers," *American Journal of Physics*, vol. 61, no. 3, pp. 242–245, Mar. 1993.

[21] T. Bai and R. W. Heath, "Coverage and rate analysis for millimeter-wave cellular networks," *IEEE Trans. Wireless Commun.*, vol. 14, no. 2, pp. 1100–1114, Oct. 2014.

[22] Q. Ma, G. D. Bai, H. B. Jing, C. Yang, L. Li, and T. J. Cui, "Smart metasurface with self-adaptively reprogrammable functions," *Light: science & applications*, vol. 8, no. 1, pp. 1–12, Oct. 2019.

[23] Q. Ma, Q. R. Hong, X. X. Gao, H. B. Jing, C. Liu, G. D. Bai, Q. Cheng, and T. J. Cui, "Smart sensing metasurface with self-defined functions in dual polarizations," *Nanophotonics*, vol. 9, no. 10, pp. 3271–3278, Apr. 2020.

[24] G. C. Alexandropoulos, N. Shlezinger, I. Alamzadeh, M. F. Imani, H. Zhang, and Y. C. Eldar, "Hybrid reconfigurable intelligent metasurfaces: Enabling simultaneous tunable reflections and sensing for 6G wireless communications," arXiv preprint arXiv:2104.04690, Apr. 2021.

[25] T. L. Jensen and E. De Carvalho, "An optimal channel estimation scheme for intelligent reflecting surfaces based on a minimum variance unbiased estimator," in *Proc. IEEE Int. Conf. on Acoust., Speech and Signal Process. (ICASSP)*, May 2020, pp. 5000–5004.

[26] R. A. Silverman *et al.*, *Special Functions and Their Applications*. Courier Corporation, 1972.

[27] G. Casella and R. L. Berger, *Statistical Inference*. Cengage Learning, 2021.

[28] R. Gatto and S. R. Jammalamadaka, "The generalized von Mises distribution," *Statistical Methodology*, vol. 4, no. 3, pp. 341–353, Jul. 2007.

[29] K. V. Mardia and S. El-Atoum, "Bayesian inference for the von Mises-Fisher distribution," *Biometrika*, vol. 63, no. 1, pp. 203–206, Apr. 1976.

[30] Z. Zhang, L. Dai, X. Chen, C. Liu, F. Yang, R. Schober, and H. V. Poor, "Active RIS vs. passive RIS: Which will prevail in 6G?" arXiv preprint arXiv:2103.15154, Mar. 2021.

[31] K. Liu, Z. Zhang, L. Dai, S. Xu, and F. Yang, "Active reconfigurable intelligent surface: Fully-connected or sub-connected?" *IEEE Commun. Lett.*, vol. 26, no. 1, pp. 167–171, Jan. 2021.

[32] J. Park Jr, "Moments of the generalized Rayleigh distribution," *Quarterly of Applied Mathematics*, vol. 19, no. 1, pp. 45–49, Apr. 1961.